ORIGINAL PAPER

Micro-scale investigation of the role of finer grains in the behavior of bidisperse granular materials

Habib Taha[1,2] · Ngoc-Son Nguyen[1] 🄳 · Didier Marot[1] · Abbas Hijazi[2] · Khalil Abou-Saleh[2]

Abstract
This paper presents a numerical study of the effect of fine content on the mechanical behavior of bidisperse granular materials using the discrete element method. Triaxial compression tests are performed on different samples with fine contents varied from 0 to 40%. It was found that, starting from 20%, fine content has a visible effect on the shear strength. The optimal fine content is about 30%, at which the shear strength is the best. An investigation into the granular micro-structure showed that the fine particles, on one hand, come into contact with coarse particles, but on the other hand, separate the latter ones as fine content increases beyond 20%. Thus, the part of the shear stress carried by the coarse–fine contacts increases, while the part carried by the coarse–coarse contacts decreases. For fine content ≤ 30%, the coarse–coarse contacts primarily carry the shear stress. Above this optimal fine content, the fine–coarse contacts overtake the coarse–coarse ones. The fine–fine contacts have little contribution to supporting the shear stress. For the studied range of fine content, the coarse particles primarily carry the shear stress, leaving the fine particles under relatively low stresses. Moreover, the matrix composed of fine particles is greatly softened by the shear loading. A classification of binary mixtures depending on their micro-structure was also proposed.

List of symbols

f_c	Fine content
f_n, f_t	Normal and tangential contact forces
K_n, K_t	Normal and tangential contact stiffnesses
k_n, k_t	Normal and tangential particle stiffnesses
E_m	Young's modulus of the particle material
φ	Contact friction angle
D_{min}, D_{max}	Minimum and maximum diameters of coarse particles
d_{min}, d_{max}	Minimum and maximum diameters of fine particles
G_r	Gap ratio
$\boldsymbol{\sigma}$	Stress tensor
p	Mean stress
q	Deviatoric stress
$\boldsymbol{\varepsilon}$	Strain tensor
ε_{11}	Axial strain
ε_v	Volumetric strain
L	Sample size
N_c	Number of coarse particles
N_f	Number of fine particles
C_v	Coefficient of variation
e	Global void ratio
n	Global porosity
e_c	Intergranular void ratio
e_f	Interfine void ratio
V_v, V_s	Void and solid volumes
F, C	Fine and coarse fractions
$C-C$	Coarse–coarse contacts
$C-F$	Coarse–fine contacts

✉ Ngoc-Son Nguyen
  ngocson.nguyen@univ-nantes.fr

  Habib Taha
  habib.taha@etu.univ-nantes.fr

  Didier Marot
  didier.marot@univ-nantes.fr

  Abbas Hijazi
  abhijaz@ul.edu.lb

  Khalil Abou-Saleh
  kabousaleh@ul.edu.lb

[1] GeM Institute, University of Nantes, 58 rue Michel Ange, BP 420, 44606 Saint-Nazaire Cedex, France

[2] MPLAB-Multidisciplinary Physics Laboratory, Faculty of Sciences, Lebanese University, Hadat-Baabda, Lebanon

$F{-}F$	Fine–fine contacts
$\mathcal{N}$	Coordination number
$\mathcal{N}_C^{C-C}$	Average number of $C{-}C$ contacts per coarse particle
$\mathcal{N}_C^{C-F}$	Average number of $C{-}F$ contacts per coarse particle
$\mathcal{N}_F^{F-F}$	Average number of $F{-}F$ contacts per fine particle
$\mathbf{f}^k$	Force at a given contact k
$\mathbf{l}^k$	Branch vector joining two particle centers at a given contact k
$\boldsymbol{\sigma}^{C-C}$	Contribution of the $C{-}C$ contacts to the macro-stress
$\boldsymbol{\sigma}^{C-F}$	Contribution of the $C{-}F$ contacts to the macro-stress
$\boldsymbol{\sigma}^{F-F}$	Contribution of the $F{-}F$ contacts to the macro-stress
ϕ^α	Volume fraction of a given phase α
$\boldsymbol{\sigma}^\alpha$	Intrinsic averaged stress of a given phase α
$\hat{\boldsymbol{\sigma}}^\alpha$	Partial stress of a given phase α
$\mathbf{M}^p$	Internal moment tensor of a given particle p
p^F, q^F	Mean and deviatoric stresses carried by the fine fraction
α	Stress reduction factor
α_p^F	Mean stress ratio for the fine fraction
α_q^F	Deviatoric stress ratio for the fine fraction
$\hat{p}^F$	Contribution of the fine fraction to the macroscopic mean stress
$\hat{q}^F$	Contribution of the fine fraction to the macroscopic deviatoric stress

1 Introduction

Granular materials are often used for construction of hydraulic earth structures such as dikes, levees, dams, etc. Granular soils with gap-graded particle-size distribution (PSD) or widely graded and upwardly concave PSD are susceptible to internal erosion, during which fine particles can be detached and transported by seepage flow through the pore space between coarse particles [1]. The migration of fine particles modifies their porosity and their micro-structure. As a consequence, internal erosion could reduce the shear strength of granular soils [2, 3], hence the stability of hydraulic earth structures. The mechanical consequence of internal erosion is still an open research topic. It requires a deep understanding of the contribution of fine particles to the mechanical behavior of granular soils.

The role of fine particles on the drained and undrained stress-strain behaviors of silty sands have been experimentally investigated [4–7]. Salgado et al. [6] observed that the drained shear strength and the dilatancy of silty sands increase with silt content. Thevanayagam et al. [7]

investigated the effect of fine content on the undrained collapse potential, which is defined as the ratio of the maximum pore pressure induced by the shear to the confining pressure. The authors found a threshold value for fine content, under which the collapse potential increases with fine content but above which it decreases with fine content. The authors attributed these opposite effects to a variation of the granular micro-structure with fine content. They made a conjecture that, with increasing fine content, the micro-structure of granular mixtures can change from a category where contacts between coarse grains are dominant to a category where contacts between fine grains are dominant. This conjecture should be verified by investigating experimentally the granular micro-structure. Such an investigation might be performed by using X-ray tomography imaging technology [8], however, this technique is quite delicate and expensive. To the best of our knowledge, no experimental investigation of the effect of fine content on the granular micro-structure has been performed so far.

Discrete element method (DEM) has been widely used to simulate numerically granular media. This method was found to be able to reproduce the main features of the mechanical behavior of granular materials such as the non-linearity, the softening phase, the dilatancy and the induced anisotropy [9]. One of its main advantages is that any local information at the particle scale can be accessed, which makes the DEM very suitable for investigating granular media from a micro-mechanical point of view. This method has been recently used by some authors to investigate the micro-structure and the micro-mechanical behavior of granular mixtures. Minh et al. [10, 11] studied the contact force distribution and the force networks in granular mixtures under one-dimensional compression. Shire et al. [12, 13] investigated the micro-structure and micro-properties of granular mixtures under isotropic compression. It is worth mentioning that a granular material subjected to a one-dimensional or an isotropic compression shows only a contractive behavior and never reaches the failure. Voivret et al. [14] studied the shear behavior and force transmission in highly polydisperse 2D granular materials composed of disks by simulating direct simple shear tests. Surprisingly, the authors found that the shear strength is almost independent of the particle size polydispersity although the solid fraction increases with the latter parameter. As the polydispersity increases, more and more large particles but less and less small particles are included in strong force chains which sustain primarily the shear stress. Dai et al. [15] also observed in their 2D simulations that fine particles leave the solid skeleton as fine content increases. In the 3D numerical simulations performed by Ng et al. [16] on binary mixtures of ellipsoids, no significant effect of fine content on the shear strength was also found. As the simulated mixtures in this study contain a few numbers of coarse particles (25, 56 and

150 for the respective fine contents 50%, 30% and 10%), the conditions required for the representative volume element are hardly fulfilled. On the contrary, Aboul-Hosn [17] found an increase of the shear strength with fine content when simulating triaxial compression tests on 3D granular mixtures with fine contents comprised between from 5% to 15%. The effect of the fine particles on the shear behavior of bidisperse granular materials at the macro- and micro-scales is apparently not well understood yet

This paper presents a numerical study of the effect of fine content on the behavior of granular mixtures under shear loading. Triaxial compression tests are simulated on granular materials with gap-graded particle size distribution by using the DEM. The performed numerical simulations are first presented in Sect. 2. The effect of fine content on the behavior of granular mixtures is then analyzed at the macro-scale as well as at the micro-scale in Sects. 3 and 4. The micro-mechanical investigation focuses on (1) the role of fine particles in the granular micro-structure, (2) the stress transmission through the contact network and the force networks in a granular mixture, and (3) the contribution of the fine particles in carrying the overburden stress. Based on this study, a classification of binary mixtures in terms of their micro-structure is proposed in Sect. 5.

2 Numerical simulations with the DEM

A dry cohesionless granular soil is an assembly of distinct particles which can be assumed to be rigid. The interaction between particles can only occur at frictional interfaces. The DEM models dry granular media as they are. This method has the two following main ingredients: (1) Newton–Euler dynamic equations to describe the translational and rotational motions of each rigid particle, and (2) a contact law to calculate the interaction forces at the contact between two particles. An explicit or implicit time-stepping scheme is used to numerically integrate the dynamic equations. At each step, the velocity and the position of each particle are integrated up to the end of the step. At the same moment, contacts between particles are detected and contact forces are calculated from the velocity and the position of particles in contact. There are two main approaches for the DEM, which differ from each other in the way of modeling the interaction at contact. The molecular dynamic (MD) approach considers a small compliance effect at the contact point so the contact force can be uniquely determined from the elastic relative displacement at the contact point [18]. On the other hand, the contact dynamic (CD) approach neglects the compliance effect at the contact point. As a consequence, the contact force cannot be uniquely determined from the relative displacement at the contact point without considering

the dynamic equations of the whole system [19]. In both approaches, Coulomb's friction law is used in the tangential direction to limit the tangential force. For the MD approach, an explicit integration scheme of high order can be used with a time step sufficiently small to describe accurately the dynamic process at the contact point. For the CD approach, the numerical integration can only be done implicitly, but with a time step much bigger than that used in the MD approach.

We use the DEM based on the MD approach, which is implemented in the open-source software YADE [20]. In this preliminary study, for the sake of simplicity, spherical particles are considered with a linear contact force-displacement model at each contact between two particles. According to this contact law, the normal and tangential interactions at a contact are modeled by two linear springs with respective stiffnesses K_n and K_t. The contact normal and tangential stiffnesses are calculated from the respective particle stiffnesses, k_n and k_t, by assuming that the latter ones are connected in series in each direction:

$$K_n = \frac{k_n^i k_n^j}{k_n^i + k_n^j} \quad \text{and} \quad K_t = \frac{k_t^i k_t^j}{k_t^i + k_t^j}, \tag{1}$$

where superscripts i and j denote two particles at the contact point. The normal particle stiffness k_n can be roughly estimated from the Young's modulus E_m of the particle material and the particle diameter D: $k_n = \pi E_m D / 2$. The tangential force f_t is limited by Coulomb friction law: $|f_t| \le f_n \tan \varphi$ where f_n is the normal force and φ is the friction angle. The microscopic parameters used in our simulations are identical to those used in the paper of Scholtès et al. [21]: normal particle stiffness $k_n / D = 250$ MPa which corresponds to $E_m = 160$ MPa, stiffness ratio $k_t / k_n = 0.5$ and friction angle $\varphi = 35°$.

Granular samples considered in this study are binary mixtures of coarse and fine particles (Fig. 1a). The particle size distribution (PSD) is a gap-graded curve as shown in Fig. 1b. This gap-graded PSD is characterized by fine content f_c and the gap ratio $G_r = D_{min}/d_{max}$ (D_{min} is the minimum diameter of coarse particles and d_{max} is the maximum diameter of fine particles). Fine content f_c is varied from 0 to 40%. A value of 3 is chosen for the gap ratio G_r to keep the computation time reasonable since a higher value of G_r leads to a large number of particles and then to a very long computation time. It is worth mentioning that, according to Chang and Zhang [22], a gap-graded soil with gap ratio of 3 might be unstable – in other words, fine particles might migrate due to seepage flow.

Particles are first generated into a cube composed of six rigid walls. At this stage, each particle diameter is reduced by a factor of 2.0. Particles are then progressively

Fig. 1 **a** A simulated granular mixture and **b** the considered gap-graded grain size distribution

(a)

(b)
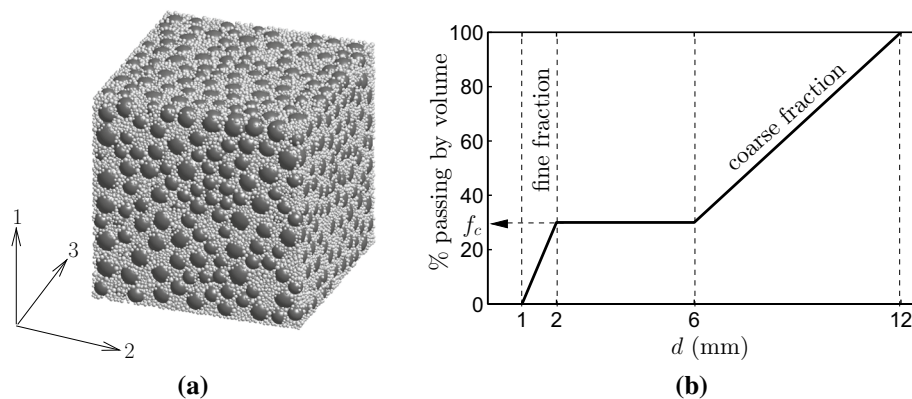
expanded to reach the target size distribution. After that, the box dimensions are slowly reduced until the stresses σ_i $(i = 1, 2, 3)$ reach a confining stress of 100 kPa. It is worth noting that 100 kPa is a typical value for the confining stress that has been often considered to perform experimentally triaxial tests on granular soils, for example by Thevanayagam et al. [7, 23], Salgado et al. [6] and Murthy et al. [4]. This value corresponds, in reality, to the horizontal stress in a dike at a depth of about 10 metres. To obtain dense samples, the friction angle φ is set to 0° during the compaction process and is then reset to its original value (35°) at the end of the compaction process. Triaxial compression tests are then performed by prescribing a small strain rate $\dot{\varepsilon}_1 = 0.01$ s^{-1} in direction (1), while keeping the lateral stresses σ_2 and σ_3 constant. Each sample is loaded until the axial strain ε_{11} reaches 15%.

Table 1 shows the number of coarse particles (N_c), the number of fine particles (N_f) and the ratio $L/D_{\max}$ of the sample size to the maximum particle diameter for different values of fine content f_c. For a given fine content, the number of coarse particles is carefully chosen such that the total number of particles is not too large and the simulated sample can be considered as a Representative Volume Element (RVE). The choice of the sample size for a gap-graded PSD is not an easy task. One might rely on experimental standards for triaxial compression tests in laboratory. For example, the ASTM standard [24] recommended that the ratio of the specimen diameter to the largest particle size is larger than 6, while the French standard [25] recommended a value larger than 5 for widely graded soils and 10 for uniformly

graded soils. It should be noted that the chosen sample sizes shown in Table 1 satisfy these criteria. For DEM numerical simulations, no clear rule has been established. Wiącek and Molenda [26] showed that for polydisperse granular packings which are not widely graded and are subjected to uniaxial compression, the RVE size is about 15 times the average particle diameter, i.e. the sample must include at least $15 \times 15 \times 15 = 3375$ particles. Salot et al. [27] found out that the RVE size for simulating a triaxial compression test on samples having a tight and uniform PSD is about 8000 particles. For a gap-graded PSD, the number of particles required for a RVE must be varied with fine content, and 8000 particles are, in general, not enough. Shire et al. [28] stated that a gap-graded sample with a minimum of 500 coarse particles can be considered as a RVE when simulating an isotropic compression. A shear loading might require a larger number of coarse particles to achieve a RVE. It is worth noting that the RVE size for a granular material is determined in a statistical sense. This means that different random generations of samples with the same size must give close results as stated by Chareyre [29]. We adopted this statistical approach to check if the simulated binary mixtures under shear loading can be considered as RVEs. For a given value of fine content f_c with the chosen sample size, five samples are randomly generated, compacted and then subjected to triaxial compression tests in the same manner. Figure 2 shows the ratio q / p of the deviatoric stress $q = \sigma_{11} - \sigma_{33}$ to the mean stress $p = (\sigma_{11} + 2\sigma_{33})/3$ and the volumetric strain ε_v versus the axial strain ε_{11} for five different samples randomly generated for $f_c = 20\%$ with the chosen sample size $L/D_{\max} = 7.2$. It

Table 1 Respective numbers, N_c and N_f, of coarse and fine particles, ratio $L/D_{\max}$ and coefficient of dispersion C_v for different values of fine content f_c

f_c (%)	N_c	N_f	$L/D_{\max}$	C_v (%)	f_c (%)	N_c	N_f	$L/D_{\max}$
0	1430	0	7.5	1.1	25	1296	93,170	7.3
5	1347	15,305	7.3	3.0	30	1246	115,186	7.4
10	1266	30,346	7.2	2.3	35	1063	123,386	7.2
15	1276	48,571	7.2	1.6	40	982	141,198	7.2
20	1273	68,646	7.2	1.7				
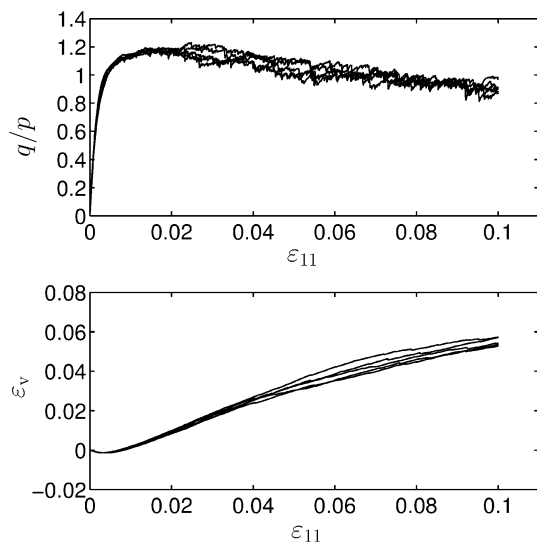
Fig. 2 Stress ratio q/p and volumetric strain ε_v versus axial strain ε_{11} for five different samples randomly generated with $f_c = 20\%$ with $L/D_{max} = 7.2$

can be seen that these five random samples with the same size show close behaviors. The dispersion in terms of shear strength (maximum value of the stress ratio q/p) is quantified by the coefficient of variation C_v used in the statistical analysis. The values of C_v for $f_c = 0$, 5%, 10% and 20% are shown in Table 1. These low values of C_v indicate that the chosen sample sizes for $f_c \leq 20\%$ can be considered as RVE sizes. For $f_c \geq 25\%$, we did not perform this repeatability study because the simulation of samples with a high fine content is very time-consuming. However, the samples with $f_c = 25\%$ and 30% can be considered as RVEs as they contain almost the same number of coarse particles as the sample with $f_c = 20\%$. For the samples with $f_c = 35\%$ and 40%, the number of coarse particles is reduced to gain the computational time while maintaining almost the same sample size. With about 1000 coarse particles, compared to the value of 500 indicated in [28], these samples can be expected to be RVEs. It is worth mentioning that the number of particles used for $f_c = 0$ is smaller than 8000 particles recommended in [27]. However, the dense state of the generated samples reduces significantly the dispersion of their behavior.

3 Macroscopic investigation

3.1 Void ratios

In a mixed soil that contains a fine content smaller than a threshold value, coarse particles may constitute a solid skeleton to carry mainly the overburden stress. A significant fraction of fine particles may be confined within pores between
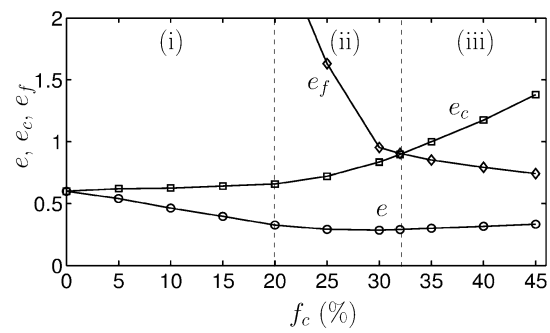

Fig. 3 Global void ratio e, intergranular void ratio e_c and interfine void ratio e_f versus fine content f_c

the former ones so they may not participate in sustaining the shear stress as stated by several authors [23, 30]. According to Thevanayagam and Mohan [23], the global void ratio, e, defined as the ratio of the volume of actual voids to the volume of solids may not be adequate to describe the density of such a mixture. The authors proposed to consider a mixed soil as a composite medium consisting of two matrices: coarse-grained matrix and fine-grained matrix. The intergranular void ratio, e_c, and interfine void ratio, e_f, were then introduced to describe the densities of the coarse-grained and fine-grained matrices, respectively. The intergranular void ratio e_c is defined by assuming that all the fine particles do not sustain any stress and can be considered as the intercoarse voids. On the other hand, the interfine void ratio e_f is defined by considering that the coarse particles are of zero volume.

$$e_c = \frac{V_v + V_s^F}{V_s^C} = \frac{e + f_c}{1 - f_c}, \quad e_f = \frac{V_v}{V_s^F} = \frac{e}{f_c}, \quad (2)$$

where V_v is the void volume; V_s^F and V_s^C are the total solid volumes of the fine particles and of the coarse particles, respectively.

Figure 3 presents the three void ratios e, e_c and e_f versus fine content f_c for the simulated samples. Three remarkable ranges of fine content with two threshold fine contents 20% and 32% can be identified. For the range (i) with $f_c < 20\%$, the intergranular void ratio e_c remains more or less constant, while the interfine void ratio e_f decreases greatly with increasing fine content f_c. This means that the fine particles fill voids left by the coarse particles without separating the latter ones. As a result, the global void ratio e decreases as fine content increases. It should be noted that the interfine void ratio e_f for this range of fine content is very high compared to the intergranular void ratio e_c and the curve for e_f cannot be fully represented in the chosen scale in Fig. 3. Within the range (ii) with $20\% \leq f_c < 32\%$, the fine particles separate the coarse ones and occupy the void space between them. The fine-grained matrix gets denser but the

coarse-grained matrix gets looser. The coarse-grained matrix is still denser than the fine-grained matrix. One would expect that there exists an intermediate configuration where the fine particles fill fully voids between coarse particles without separating them; however, this is not the case. As shown in Fig. 3, at $f_c = 20\%$, fine particles begin to separate coarse ones but the interfine void ratio e_f is still very large. This means that intercoarse voids are not fully filled yet by the fine particles. It is interesting to note that, at the last threshold fine content $f_c = 32\%$, the interfine void ratio e_f is equal to the intergranular one e_c, and the global void ratio e reaches it minimum value. Lade et al. [31] also observed an optimal fine content at which the global void ratio is minimum when analyzing experimentally the density of mixtures of coarse and fine spherical balls. In these experiments, equal coarse balls of diameter D are mixed with equal fine balls of diameter d. The coarse balls are deposited first in a container and the fine balls are then added from the top while the container is vibrated. For mixtures with the ratio $D/d = 3.5$, the optimal fine content is about 40%. It should be noted that the difference between the optimal fine content of 32% found in our study and the value of 40% shown in [31] may be related to the fact that the coarse balls, as well

as the fine balls, are of different size and they are generated and compacted simultaneously in our study. In doing so, the fine balls have more chance to be intercalated between the coarse particles. Minh et al. [11] also found an optimal fine content of about 30% in their simulations of binary mixtures. Figure 3 also shows that, for the range (iii) where fine content goes beyond 32%, the coarse particles are greatly separated by the fine ones and the coarse-grained matrix gets looser than the fine-grained matrix.

3.2 Stress–strain behavior

Figure 4 shows the stress ratio q / p and the volumetric strain ε_v versus the axial strain ε_{11} for the simulated samples. The macroscopic Young's modulus, E, for each sample is defined as the initial slope of the corresponding stress-strain curve for the range of the axial strain from 0 to 0.1%. The maximum and residual values of the macroscopic friction angle, ϕ_{peak} and $\phi_{residual}$, are also calculated using the Morh-Coulomb yield criterion. Table 2 shows these macroscopic properties for different values of fine content. It is shown that the macroscopic Young's modulus is lower than the microscopic one ($E_m = 160$ MPa) given to the numerical model

Table 2 Macroscopic Young's modulus, E, maximum and residual values of the macroscopic friction angle, ϕ_{peak} and $\phi_{residual}$, for different values of fine content f_c

f_c (%)	0	5	10	15	20	25	30	32	35	40
E (MPa)	77	69	72	67	69	78	120	137	77	85
ϕ_{peak} (°)	28	28	29	30	33	37	40	40	37	36
$\phi_{residual}$ (°)	21	20	22	19	21	17	15	12	11	15
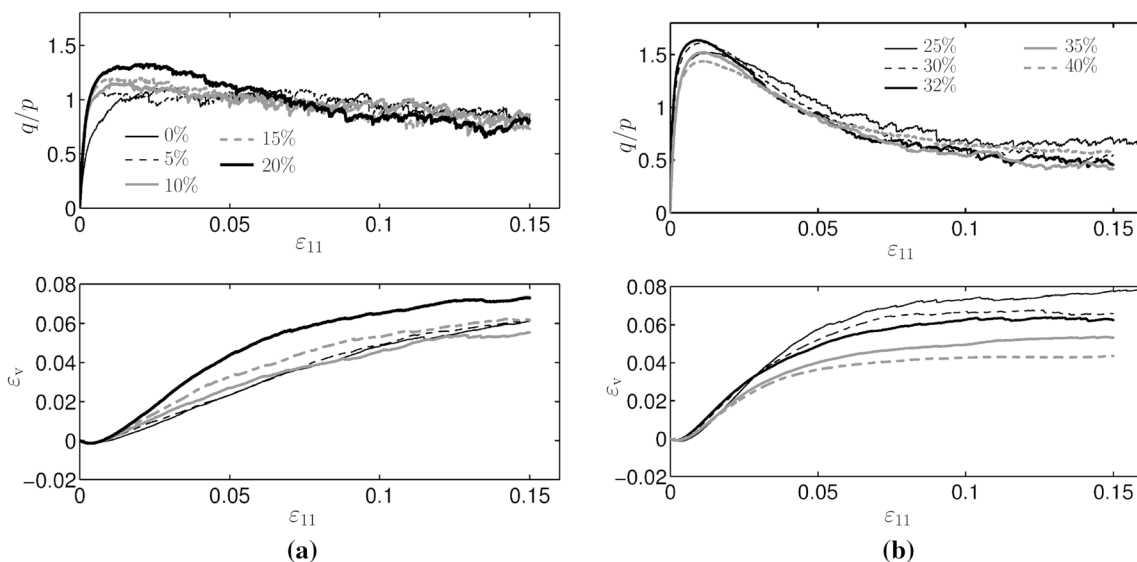
Fig. 4 Stress ratio q / p and volumetric strain ε_v versus axial strain ε_{11} for different values of fine content: **a** f_c varies from 0 to 20% and **b** f_c varies from 25% to 40%

presented in Sect. 2 whatever fine content f_c. Holtzman et al. [32] found a similar result in their simulations with Hertzian contact model. This is consistent with the fact that a sand sample, which is composed of distinct solid particles and voids, cannot be stiffer than sand solid particles. On the other hand, a sand sample might have a better shear resistance than individual contacts between sand particles. As shown in Table 2, the macroscopic friction angle at the peak state is indeed higher than the microscopic one ($\varphi = 35°$) for fine contents $f_c \geq 25\%$. In fact, the macroscopic shear strength depends not only on the microscopic friction angle but also on several other factors such as particle shape, particle packing and arrangement [33–35]. One can also remark in Table 2 that the macroscopic residual friction angle is quite low compared to the microscopic one whatever fine content f_c.

Figure 4 shows that fine content f_c does not significantly affect the stress-strain behavior of the granular mixtures with $f_c < 20\%$ but it does for $f_c \geq 20\%$. There exists an optimal fine content f_c of 32% under which the macroscopic Young's modulus and the shear strength at the peak state increase with f_c but above which the latter macroscopic properties decrease with f_c (Fig. 4b; Table 2). It is interesting to note that the optimal fine content of 32% found here is also the threshold value observed in Fig. 3 at which the intergranular and interfine void ratios are equal and the global void ratio is minimum. The same tendency is observed for the material dilatancy except that the threshold fine content for it is about 35%, which is also quite close to the value of 32% observed for the maximum shear strength. As the stress-strain curve for $f_c = 32\%$ is almost coincident with the one for $f_c = 30\%$, we consider that the second fine content threshold is 30% instead of 32% and we do not show the results obtained with $f_c = 32\%$ in the following.

The above results mean that a reasonable fine content ($20\% \leq f_c \leq 30\%$) can make granular materials stronger and more dilatant. This is in good agreement with the experimental results of Salgado et al. [6] who performed drained triaxial tests on mixtures of clean Ottawa sand and silt. In this study, the effect of fine particles was clearly observed even at a low fine content ($f_c \leq 15\%$). This might be explained by the fact that the sand-silt mixtures considered in their study have continuous and broadly graded PSDs, for which fine particles might fill the void space between coarse particles even at low fine content. Figure 4b also shows that a too high fine content ($f_c > 30\%$) can be a factor unfavorable to the shear strength and dilatancy of granular mixtures. The mixture with $f_c = 40\%$ has indeed a lower shear strength and a lower dilatancy than the mixture with $f_c = 30\%$.

A dense granular sample exhibits a peak on the stress-strain curve, followed by a marked softening phase. This kind of behavior can be observed for the mixtures with $f_c \geq 20\%$. The critical state is an important concept in soils mechanics, at which soils deform without any change in their volumetric strain and their shear strength. Soils reach, in general, this particular state at large strain. In our simulations, we perform triaxial tests until 15% of the axial strain, which is the value recommended by the the ASTM standard [24]. As shown in Fig. 4, the simulated samples reach almost the critical state. As shown in Fig. 4b and Table 2, the fine particles, on one hand, strengthen granular mixtures at the peak state, but on the other hand, weaken them at the critical state. Indeed, the macroscopic friction angle for $f_c = 30\%$ is 15° at the critical state, much lower than the value of 40° at the peak state.

One could try to explain the effect of fine content on the mechanical behavior of granular mixtures by using the dependency of the void ratios e, e_c and e_f upon fine content f_c shown in Fig. 3. The negligible effect of the fine particles on the stress-strain behavior observed for the mixtures with $f_c < 20\%$ is related to the fact that the fine-grained matrix is very loose (range (i) in Fig. 3) so the fine particles do not participate actively in supporting the external loading. However, it is not easy to explain why the shear strength and the dilatancy increase with fine content when $f_c > 20\%$ but decrease when $f_c > 30\%$, and why a mixture with a significant fine content shows a marked softening phase. It should be noted that adding fine particles into a mixture leads to two opposing effects: on one hand, the coarse-grained matrix gets looser, which weakens the mixture, but on the other hand, the fine-grained matrix gets denser, which strengthens the mixture. It is not well understood yet which effect is more important than the other for a given fine content. In the following, we bring some insights into granular mixtures to better understand how the fine particles modify the granular micro-structure and participate in sustaining the applied shear stress.

4 Microscopic investigation

In this section, we first define three coordination numbers to describe the micro-structure of granular mixtures and then show how they depend on fine content and how they evolve during shear loading. Next, the transmission of the shear stress through the contact network and the composition of force chains are analyzed. Finally, we show how the fine-grained and coarse-grained matrices participate in carrying the shear stress.

4.1 Coordination numbers

Coordination number, denoted by $\mathcal{N}$, is defined as the average number of contacts per particle. It is usually used to describe the density of a granular assembly at the micro-scale. However, this definition of the coordination number

is not appropriate for a mixture of coarse and fine particles because the number of contacts per coarse particle is very different from that per fine particle. As mentioned previously, a binary granular mixture can be thought of as a multi-phase medium which is composed of the coarse-grained matrix, the fine-grained matrix and the interface between them. The interaction between particles in each phase occurs through $C-C$ contacts (between two coarse particles), $F-F$ contacts (between two fine particles), respectively; and these two phases interact each other through $C-F$ contacts (between a coarse and a fine particle). Describing the local densities of the coarse-grained and fine-grained matrices and of the interface between them needs thus three coordination numbers, denoted by $\mathcal{N}_C^{C-C}$, $\mathcal{N}_F^{F-F}$ and $\mathcal{N}_C^{C-F}$, which are defined as the respective average numbers of $C-C$ contacts per coarse particle, of $F-F$ contacts per fine particle, and of $C-F$ contacts per coarse particle. Minh and Cheng [36] and Shire et al. [13, 37] also defined similar coordination numbers to study the micro-structure of granular mixtures.

Figure 5a–c shows the respective coordination numbers $\mathcal{N}_C^{C-C}$, $\mathcal{N}_C^{C-F}$ and $\mathcal{N}_F^{F-F}$ versus fine content f_c at the initial, peak and critical states. It can be seen that, at the initial state, the coordination number $\mathcal{N}_C^{C-C}$ remains more or less constant and the coordination numbers $\mathcal{N}_F^{F-F}$ and $\mathcal{N}_C^{C-F}$ are very small for $f_c < 20\%$. This confirms the statement made in Sect. 3.1 that the fine particles are almost floating

(a)

(b)

(c)

Fig. 5 Coordination numbers **a** $\mathcal{N}_C^{C-C}$, **b** $\mathcal{N}_C^{C-F}$ and **c** $\mathcal{N}_F^{F-F}$ versus fine content f_c at the initial, peak and critical states

within voids between coarse ones and they do not modify the granular skeleton which is mainly constituted of coarse particles. Starting from $f_c = 20\%$, a further addition of fine particles leads, on the whole, to a strong increase in $\mathcal{N}_C^{C-F}$ and $\mathcal{N}_F^{F-F}$, particularly for $\mathcal{N}_C^{C-F}$, but to a remarkable decrease in $\mathcal{N}_C^{C-C}$. This means that an increase in fine content induces two opposing effects. On one hand, fine particles disrupt contacts between coarse ones so they weaken the coarse fraction. On the other hand, a significant quantity of fine particles around each coarse particle reinforce the interface between the coarse-grained and fine-grained matrices. Furthermore, more contacts between fine particles are created so the fine-grained matrix gets stronger. Shire et al. [37] also observed a decrease in number of contacts par coarse particle and an increase in number of contacts per fine particle with increasing fine content for granular mixtures with bigger values of the gap ratio G_r. The best shear strength at the peak state for $f_c = 30\%$ shown in Fig. 4b can be attributed to the fact that the coarse particles are strongly reinforced by an important number of fine particles around them (about 50 fine particles per coarse particle, on average), despite the fact that they are slightly weakened by a loss of contacts between them.

Figure 5 also shows a remarkable decrease in the coordination numbers $\mathcal{N}_C^{C-C}$, $\mathcal{N}_C^{C-F}$ and $\mathcal{N}_F^{F-F}$ at the peak and critical states for the samples with $f_c > 20\%$. The most drastic drop in $\mathcal{N}_C^{C-C}$, $\mathcal{N}_C^{C-F}$ and $\mathcal{N}_F^{F-F}$ is observed for $f_c = 30\%$: $\mathcal{N}_C^{C-C}$ and $\mathcal{N}_C^{C-F}$ decrease from 3.8 and 44.9 at the initial state to 1.8 and 9.1 at the critical state, respectively. This drastic drop in the coordination numbers means that the micro-structure of these samples is strongly altered after the peak state, which explains why they exhibit a marked softening phase as shown in Fig. 4.

The next section gives us more insights into how the shear stress is transmitted through the coarse–coarse, coarse–fine and fine–fine contacts in granular mixtures.

4.2 Stress transmission through the contact network

When a granular sample is subjected to an external loading, contacts between particles participate in transferring forces [38, 39]. The stress tensor defined at the macro-scale can be related to contact forces at the micro-scale by using the following static homogenization operator [40]:

$$\sigma_{ij} = \frac{1}{V} \sum_k f_i^k l_j^k. \tag{3}$$

The stress tensor $\boldsymbol{\sigma}$ is defined on a volume V whose boundary is tangent to the particles that are close to it (Fig. 6). Superscript k runs over not only all contacts between particles (interior contacts) but also all contacts between particles
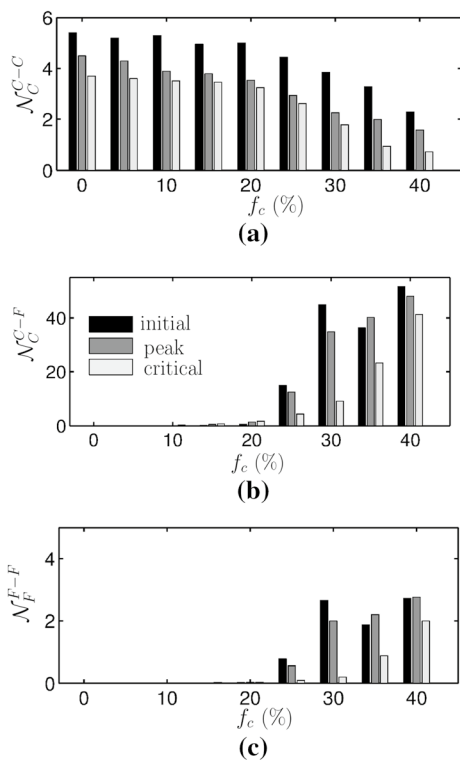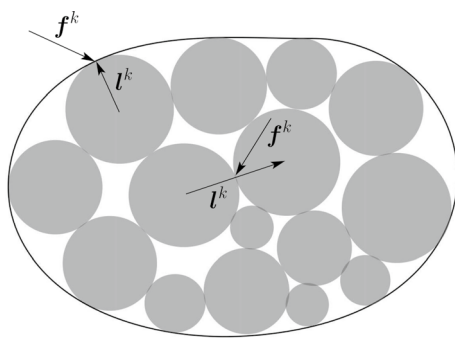
Fig. 6 Illustration of a volume on which the stress tensor σ is defined
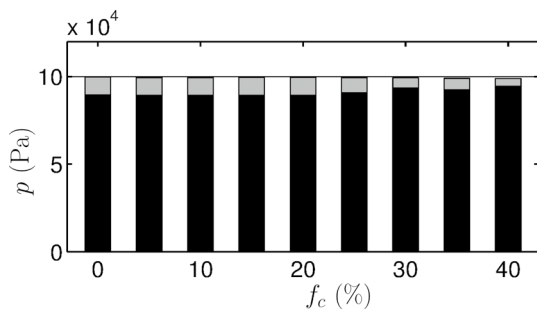

Fig. 7 The mean stress p estimated with (3) at the initial state is compared to the mean stress $p = 100$ kPa applied on the boundary of samples with different values of fine content f_c. Black and gray colors represent the contributions of the interior contacts and of the contacts on the boundary, respectively

and the boundary. For a contact between two particles, f^k is the contact force and l^k is the branch vector joining two particle centers at this contact. For a contact between a particle and the boundary, f^k is the force exerted by the exterior to the particle and the vector l^k joins the particle center to the contact point.

It has been well known in the literature that the static homogenization operator (3) gives a good estimation of the macroscopic stress tensor if the volume under consideration contains a sufficient number of particles. This can be confirmed in Fig. 7 where the mean stress p estimated with (3) is compared to the value of 100 kPa applied on the boundary at the initial state for different values of fine content f_c. Figure 7 also shows that the contribution of the contacts on the boundary (the rigid walls in our simulations) to the macroscopic stress tensor σ is not negligible (about 10% for $f_c \leq 20\%$) and it decreases as fine content f_c increases (about 4.5% for $f_c = 40\%$). This is due to the fact that the sample sizes L chosen for the simulated samples (Table 1) are not too large compared to the maximum particle size D_{max} so the number of contacts on the boundary is not negligible compared to the number of interior

contacts. It is expected that the stress part relative to the contacts on the boundary is negligible compared to that relative to the interior contacts when the sample size is big enough compared to the particle size. The contacts on the boundary result indeed in no more than 2% of the macro-stress for a sample of $f_c = 0$ with $L/D_{max} = 38$.

The stress part relative to the contacts between particles can be split into three parts σ^{C-C}, σ^{C-F} and σ^{F-F} which correspond to the contributions of the respective categories of $C-C$, $C-F$ and $F-F$ contacts. For example, the contribution of the set of $C-C$ contacts to the stress tensor σ is computed as:

$$\sigma_{ij}^{C-C} = \frac{1}{V} \sum_{k \in C-C} f_i^k l_j^k. \tag{4}$$

The stress tensors σ^{C-C}, σ^{C-F} and σ^{F-F} have the same principal directions as those of the macro-stress tensor σ. The contributions of each category of contacts to the macroscopic mean and deviatoric stresses, p and q, can be calculated, for example $p^{C-C} = (\sigma_{11}^{C-C} + 2\sigma_{33}^{C-C})/3$ and $q^{C-C} = \sigma_{11}^{C-C} - \sigma_{33}^{C-C}$. Minh et al. [11] used the same stress decomposition to study the contributions of each category of contacts to the macro-stress for binary mixtures under one-dimensional compression.

The mean and deviatoric stresses calculated for the three categories of contacts are plotted versus the axial strain ε_{11} in Fig. 8a, b for $f_c = 20\%$ and 30%, respectively. Their values at the peak and critical states are plotted versus fine content f_c in Fig. 9. It is shown that, for $f_c < 20\%$, the $C-F$ and $F-F$ contacts do not contribute significantly to the macro-stress. For instance, for $f_c = 15\%$, all the $C-F$ contacts contribute to only 4% of the macroscopic mean and deviatoric stresses at the peak state. A major part of the macro-stress is carried by the $C-C$ contacts and it remains more or less constant for $f_c < 20\%$. This is in agreement with the result shown in Fig. 5 where the coordination numbers $\mathcal{N}_C^{C-F}$ and $\mathcal{N}_F^{F-F}$ are negligible compared to $\mathcal{N}_C^{C-C}$ which is not affected by a low fine content. Starting from $f_c = 20\%$, the $C-F$ contacts contribute to supporting the shear stress. For this threshold value, the $C-F$ contacts carry about 10% of the macro-stress despite a low value of $\mathcal{N}_C^{C-F}$, while the stress part carried by the $C-C$ contacts is almost the same as that for the samples with $f_c < 20\%$ (Figs. 8a, 9). This explains why the effect of fine content on the shear strength is visible starting from 20% (Fig. 4). It is worth mentioning that it is not easy to explain this if we look only at the void ratios in Fig. 3 and at the coordination numbers in Fig. 5.

The $C-F$ and $F-F$ contacts participate more and more in sharing the macro-stress as f_c increases from 20% as shown in Fig. 9. At $f_c = 30\%$, the $C-F$ contacts actually contribute to the deviatoric stress q as much as the $C-C$
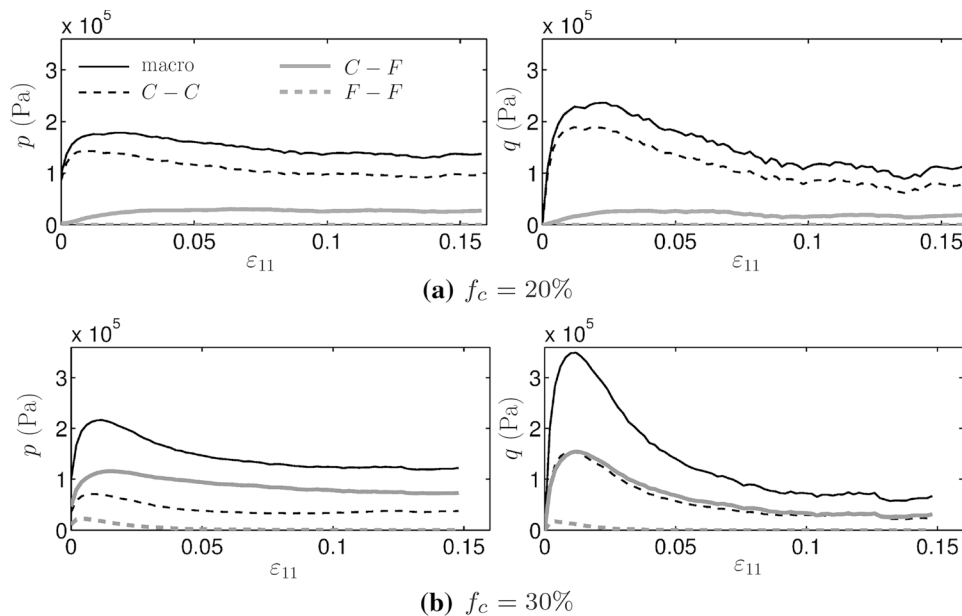
Fig. 8 Contributions of the three categories of $C{-}C$, $C{-}F$ and $F{-}F$ contacts to the macroscopic mean and deviatoric stresses, p and q, versus axial strain ε_{11} for **a** $f_c = 20\%$ and **b** $f_c = 30\%$

(a) $f_c = 20\%$

(b) $f_c = 30\%$

Fig. 9 Contributions of the three categories of $C{-}C$, $C{-}F$ and $F{-}F$ contacts to the macroscopic mean and deviatoric stresses, p and q, versus fine content f_c at the peak state (**a**, **b**) and at the critical state (**c**, **d**)

(a) p at the peak state

(b) q at the peak state

(c) p at the critical state

(d) q at the critical state
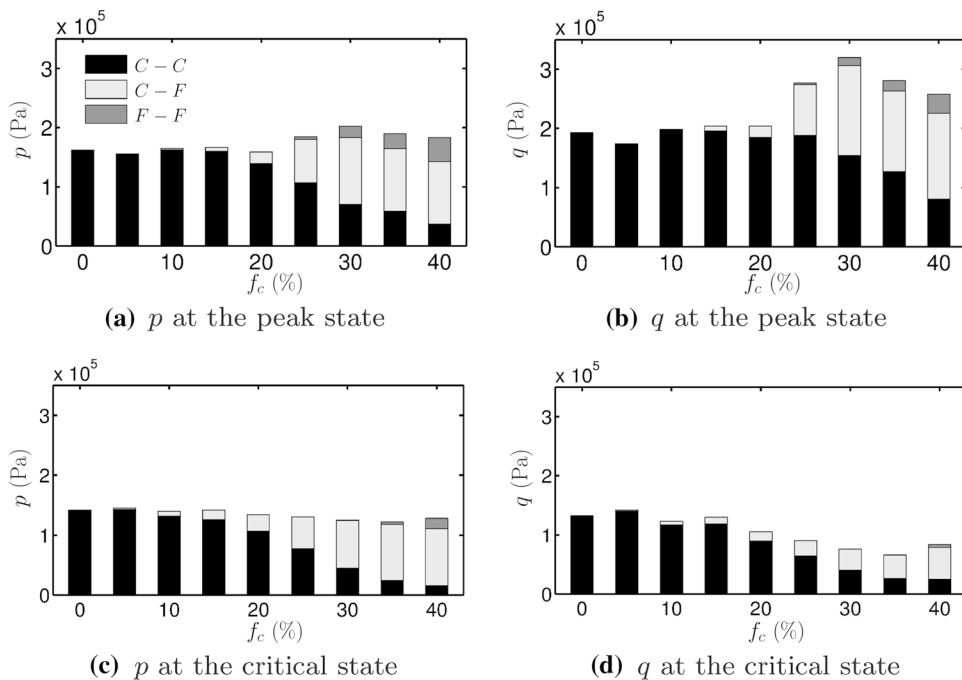
contacts. Interestingly, they contribute even more to the mean stress p than the latter ones (see also Fig. 8b). The role of the $C{-}F$ contacts becomes more important than the role of the $C{-}C$ contacts at $f_c = 40\%$ at which the former ones contribute to about 53% of the deviatoric stress q at the peak state, compared to a value of 35% for the latter ones. The $F{-}F$ contacts have a visible contribution to the macro-stress at the peak state when $f_c \geq 30\%$; however, their contribution is quite small, compared to those of the $C{-}C$ and $C{-}F$ contacts. At $f_c = 40\%$, the $F{-}F$ contacts contribute to 22% of the mean stress p and to 12% of the

deviatoric stress q. The increasing role of the $C{-}F$ and $F{-}F$ contacts and the decreasing role of the $C{-}C$ contacts with increasing fine content from 20% are related to the increase in the coordination numbers $\mathcal{N}_C^{C{-}F}$ and $\mathcal{N}_F^{F{-}F}$, and to the decrease in the coordination number $\mathcal{N}_C^{C{-}C}$ (Fig. 5), respectively. One can remark that the $C{-}C$ and $C{-}F$ contacts reverse their roles in sustaining the shear stress at the threshold fine content of 30%: above this value, the $C{-}F$ contacts sustain more the shear stress than the $C{-}C$ contacts. The contribution of the $C{-}F$ contacts to the macro-stress increases quickly with $f_c \leq 30\%$,

which compensates a decrease in the contribution of the $C-C$ contacts. As a consequence, the shear strength at the peak state increases with fine content $f_c \leq 30\%$. However, an increase in fine content f_c from 30% does not lead to a significant increase in the stress part carried by the $C-F$ contacts but leads to a strong decrease in the stress part carried by the $C-C$ contacts. Consequently, the shear strength at the peak state decreases with fine content $f_c > 30\%$. It is interesting to note that Minh et al. [11] also observed a transition at 30% of fine content for binary mixtures subjected to one-dimensional compression with a gap ratio of 4.0, above which the $C-F$ contacts overtake the $C-C$ contacts in carrying the shear stress. The authors also showed that at a very high fine content ($f_c > 60\%$), the coarse particles are strongly dispersed by the fine particles; in this case the major contribution to the shear stress is provided by the $F-F$ contacts.

Figure 9 also shows a marked decrease in the deviatoric stresses supported by the three categories of contacts at the critical state for the samples with $f_c \geq 30\%$. The most drastic drop is observed for the sample with 30% of fine content where the deviatoric stresses supported by the $C-C$ and $C-F$ contacts are reduced by a factor > 3 from the peak state to the critical state. As a consequence, its shear strength is greatly reduced at the critical state, which is consistent with the great degradation of its micro-structure after the peak state as shown in Fig. 5. The deviatoric stress carried by the $C-C$ contacts for the sample with $f_c = 30\%$ becomes much lower than that for the sample with $f_c = 0$ at the critical state. In addition, the $C-F$ contacts in the former sample suffer a great softening phase. This explains why the residual shear strength for $f_c = 30\%$ is lower than that for $f_c = 0$ (Table 2). It is worth noting in Fig. 9 that the mean stress at the critical state is primarily carried by the $C-F$ contacts for $f_c \geq 30\%$, and the $F-F$ contacts carry almost no stress at this state.

We have shown in this section that the external stress applied to a binary mixture is mainly transmitted through the $C-C$ and $C-F$ contacts. It does not mean that all the $C-C$ or $C-F$ contacts carry in the same manner the external stress since force transmission through a granular medium is well known to be very heterogeneous. In the same system, there exist strong and weak force networks with different roles in sustaining the shear stress. In the next section, we analyze how the contacts in each category constitute the strong and weak force networks.

4.3 Strong and weak force networks

According to the definition of Radjai and Wolf [38], the weak and strong force networks are composed of the contacts where the contact force f^c is smaller and bigger than the average contact force $\bar{f}$, respectively. The authors found
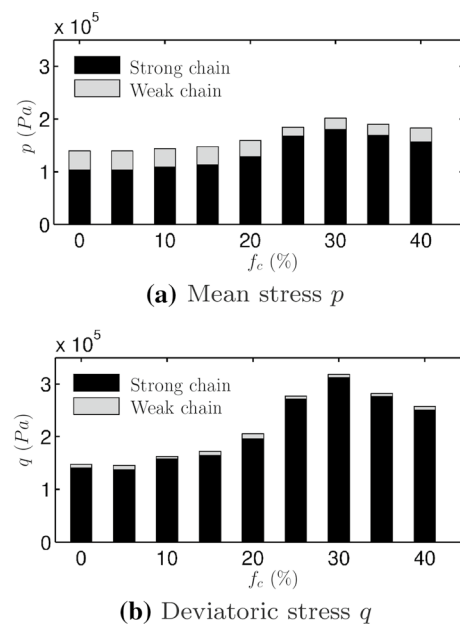

(a) Mean stress p

(b) Deviatoric stress q

Fig. 10 Contributions of the strong and weak force chains to the mean stress p and the deviatoric stress q versus fine content f_c
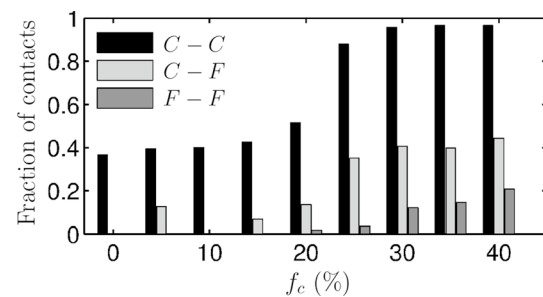

Fig. 11 Fraction of $C-C$, $C-F$ and $F-F$ contacts in the strong network at the peak state

that the strong network sustains almost the shear stress and the weak network behaves like a liquid without bearing any shear stress. The same result is obtained for the binary mixtures considered in this study as shown in Fig. 10. It can be seen that the weak network sustains a negligible part of the deviatoric stress q.

Figure 11 shows the fractions of $C-C$, $C-F$ and $F-F$ contacts in the strong network versus fine content f_c at the peak state. For instance, the fraction of $C-C$ contacts in the strong force network is defined as the ratio of the number of $C-C$ contacts in the strong force network to the total number of $C-C$ contacts. It can be seen that, at low fine content ($f_c < 20\%$), the strong force network is constituted of about 40% of $C-C$ contacts and a much smaller fraction of $C-F$ contacts. As fine content increases, more $C-C$ contacts participate in the strong force network. More than 95% of $C-C$ contacts actually take part in the strong force network for $f_c \geq 30\%$. Voivret et al. [14]

also showed that the strong force network passes preferentially through coarse particles in highly polydisperse samples. This result can be explained by the fact that the presence of fine particles around coarse ones makes contacts between coarse particles stronger so they carry a much bigger force. It does not mean, however, that the $C-C$ contacts can carry a bigger stress: they carry, indeed, a lower stress at $f_c = 30\%$ than at $f_c = 10\%$ (Fig. 9) because more $C-C$ contacts are disrupted by fine particles at $f_c = 30\%$. Figure 11 also shows that an increasing fraction of $C-F$ and $F-F$ contacts take part in the strong force network as fine content increases so they sustain more the shear stress. However, a major fraction of these contacts are located in the weak force network (more than 56% of $C-F$ contacts and 80% of $F-F$ contacts). This is also true for binary mixtures under one-dimensional compression at very high fine content ($f_c > 70\%$) as shown by Minh et al. [11].

The above analyzes have shown how the macroscopic stress is transmitted through the contact network in a granular mixture but they do not show how much stresses the coarse-grained and fine-grained matrices carry. According to Skempton and Brogan [30], the stress carried by the fine fraction is an important factor that influences the susceptibility of a granular material to internal erosion. In the next section, we define first the stresses carried by each matrix, and then we show how they depend on fine content.

4.4 Stresses carried by the fine and coarse fractions

In addition to the coarse-grained matrix (C) and the fine-grained matrix (F) in a granular mixture, voids (V), which can be filled by water or not, are present between solid particles. By homogenizing the stress field in this heterogeneous medium, the macroscopic stress can be defined from its counterpart within each phase:

$$\sigma_{ij} = \sum_{\alpha \in \{F,C,V\}} \phi^\alpha \sigma_{ij}^\alpha = \sum_{\alpha \in \{F,C,V\}} \hat{\sigma}_{ij}^\alpha. \tag{5}$$

For each phase α, ϕ^α is its volume fraction, i.e. the ratio of its volume V^α to the total volume V. The *intrinsic averaged stress* σ^α is defined as the average of the microscopic stress field $\sigma(x)$ which prevails in the phase under consideration:

$$\sigma_{ij}^\alpha = \frac{1}{V^\alpha} \int_{x \in V^\alpha} \sigma_{ij}(x) dV. \tag{6}$$

According to the mixture theory, the tensor $\hat{\sigma}^\alpha = \phi^\alpha \sigma^\alpha$ is called *partial stress*, which can be understood as the contribution of the phase under consideration to the macroscopic stress σ. It should be noted that it is the intrinsic averaged stress σ^α that gives information on how much the phase under consideration is stressed. For a dry mixture, voids bear zero-stress so we obtain:

$$\sigma_{ij} = \phi^F \sigma_{ij}^F + \phi^C \sigma_{ij}^C = (1-n)\left[f_c \sigma_{ij}^F + (1-f_c)\sigma_{ij}^C\right]. \tag{7}$$

The volume fraction ϕ^F of the fine fraction is related to fine content f_c and the porosity n by $\phi^F = (1-n)f_c$.

Using the definition (6) with some transformations, one can define the intrinsic averaged stresses σ^F and σ^C in the fine and coarse fractions as follows:

$$\sigma_{ij}^F = \frac{1}{V_s^F} \sum_{p \in F} M_{ij}^p, \quad \sigma_{ij}^C = \frac{1}{V_s^C} \sum_{p \in C} M_{ij}^p, \tag{8}$$

where superscript p runs over all the particles in each fraction; and V_s^F and V_s^C are the respective total solid volumes of the fine and coarse fractions. The tensor M^p, called *internal moment tensor* by Moreau [41], is defined for each particle p as follows:

$$M_{ij}^p = \sum_{k \in p} f_i^k r_j^k \tag{9}$$

where superscript k denotes each contact on the particle under consideration; the vector r^k connects the particle center to the contact point; and f^k is the contact force. As stated in [41, 42], the physical meaning of the internal moment tensor M^p remains the same when it is applied to a single particle or when it is applied to a collection of particles. Moreover, when it is applied to a large scale, i.e. a collection contains a large number of particles, its physical meaning tends to that of the Cauchy stress tensor. It should be noted that the estimated macroscopic stress tensor defined by (3) can be recovered by summing the tensors M^p over all the particles:

$$\sigma_{ij} = \frac{1}{V} \sum_p M_{ij}^p. \tag{10}$$

The definition (8) can also be transformed to

$$\sigma_{ij}^F = \frac{1}{V_s^F} \sum_{p \in F} \sigma_{ij}^p V_s^p, \quad \sigma_{ij}^C = \frac{1}{V_s^C} \sum_{p \in C} \sigma_{ij}^p V_s^p, \tag{11}$$

where σ^p is the stress tensor defined for each particle with the solid volume V_s^p: $\sigma^p = M^p / V_s^p$.

Inspired from the stress reduction factor α for the fine fraction that was introduced by Skempton and Brogan [30], we define two stress factors α_p^F and α_q^F, which are the respective ratios of the mean and deviatoric stresses carried by the fine fraction, p^F and q^F, to their macroscopic counterparts, p and q

$$\alpha_p^F = p^F / p, \quad \text{and} \quad \alpha_q^F = q^F / q, \tag{12}$$

where p^F and q^F are computed from the intrinsic averaged stress tensor σ^F defined by (8). The defined stress factors α_p^F and α_q^F can be thought of as being the relative mean and deviatoric stresses carried by the fine fraction, compared to the macroscopic counterparts. It is worth mentioning that if both fractions carried the same stress, these two stress

factors would be $\alpha_p^F = \alpha_q^F = 1/(1-n)$. Shire et al. [28] defined a stress reduction factor $\alpha = p^F/p$ for the fine fraction. The authors computed the averaged stress σ^F in the fine fraction using the definition (11). However, instead of considering the solid volume V_s^p of each particle, the authors associated to each particle an amount of void surrounding it, so the volume considered for each particle when computing the averaged stress σ^p is $V^p = V_s^p/(1-n)$. By doing so, a binary mixture is considered as a biphasic material: the fine and coarse fractions with the respective total volumes $V^F = V_s^F/(1-n)$ and $V^C = V_s^C/(1-n)$. As a consequence, the resulting stress tensor σ^F is no longer intrinsic to the solid fraction of the fine particles according to (6) and the resulting stress factor α is lower than that defined in the current study.

Figure 12 shows the absolute mean and deviatoric stresses carried by the fine and coarse fractions versus fine content f_c at the initial, peak and critical states. The stress factors α_p^F and α_q^F for the fine fraction are shown in Fig. 13. It can be seen that at a low fine content ($f_c < 20\%$), the fine fraction carries almost zero-stress. This confirms that the fine particles are almost floating in voids between coarse particles and carry low stresses. According to Skempton and Brogan [30], a significant proportion of fine particles in this case can be easily washed out by water flow even

at low hydraulic gradient – in other words, these mixtures are internally unstable. It should be noted that a low stress carried by the fine fraction is just a necessary condition for the internal instability. This just means that fine particles can be easily detached by water flow. The sufficient condition is whether or not the primary fabric formed by solid particles allow detached fine particles to migrate within the interstices of this framework.

At a higher fine content ($f_c \geq 20\%$), the fine particles participate in carrying the applied stress, and its participation increases with fine content. It is interesting to note in Fig. 13 that the fine fraction plays a more important role in carrying the mean stress than in carrying the deviatoric stress: at $f_c = 40\%$, $\alpha_p^F = 1.0$ compared to $\alpha_q^F = 0.6$ at the peak state. Shire et al. [28] also found that the stress factor α at the isotropic stress state increases with fine content; moreover it depends significantly on the gap ratio G_r. By investigating the stress factors α_p^F and α_q^F during the shear loading, we find that the shearing leads to a significant reduction in the stress carried by the fine fraction (Fig. 13). For the mixture with $f_c = 30\%$, which exhibits the most marked softening behavior as shown in Fig. 4, the stress factor α_p^F reduces indeed from 0.84 at the initial state to 0.43 at the critical state. This result indicates that the fine fraction is greatly softened by the shear loading, which might make them more vulnerable to internal erosion. Concerning the coarse

Fig. 12 The mean stress **a** p and the deviatoric stress **b** q carried by the fine and coarse fractions, compared to the macroscopic ones, versus fine content f_c at the peak state
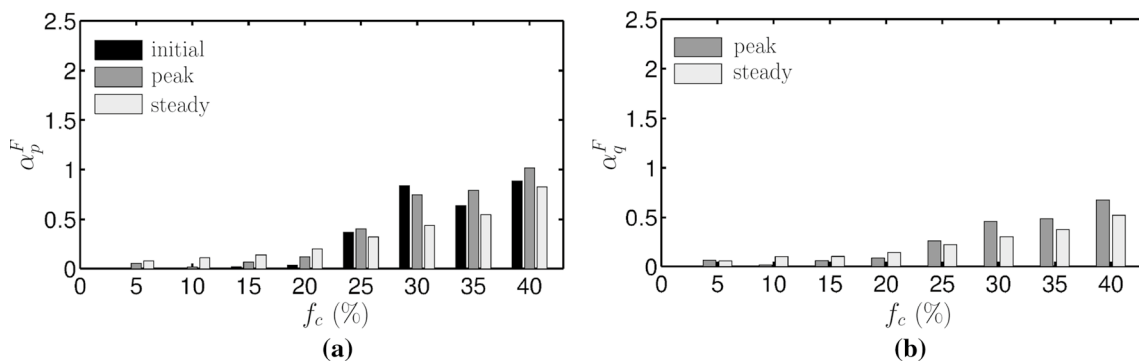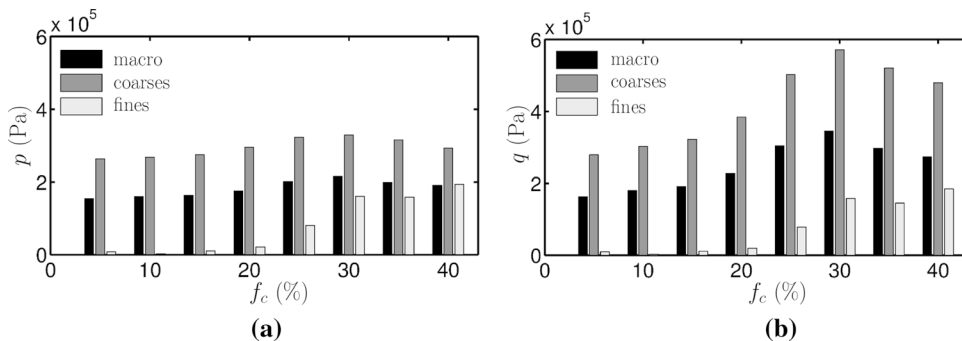

Fig. 13 Stress factors **a** α_p^F and **b** α_q^F defined for the fine fraction versus fine content f_c at the initial, peak and critical states

fraction, since voids do not carry any stress and the fine fraction carries a stress smaller than the macroscopic stress, it carries a stress much bigger than the macroscopic stress. As shown in Fig. 12, the stress carried by the coarse fraction is indeed about 1.6 times the macroscopic stress. Furthermore, it increases with fine content for $f_c \leq 30\%$ but decreases for $f_c > 30\%$ (Fig. 12). This result confirms the optimal fine content $f_c = 30\%$ under which the coarse fraction is reinforced by fine particles but above which the coarse fraction is weakened since fine particles strongly separate them.

Let us now give an explanation of why the coarse fraction gets stronger as fine content f_c increases between 20% and 30%. Solid particles with frictional surface can be thought of as gears in a mechanical transmission system so a granular binary sample can be assimilated to a system of small gears and big gears (Fig. 14). Black and gray gears correspond to the particles included in the strong and weak force networks, respectively. For $f_c \leq 30\%$, the strong force network is primarily constituted of big gears. In such a system, small gears have the two following important roles. Firstly, small gears intercalated between strong force columns serve as a bracing system to laterally stabilize the latter ones: without them, strong force columns would collapse. Secondly, an important number of small gears around big gears wedge the latter ones, thus prevent greatly their rotation. In this case, sliding and rolling at contacts between big gears are greatly reduced; thus, the coarse fraction gets stronger and the shear strength of granular mixtures increases with increasing fine content. Indeed, Calvetti et al. [43] and Belheine et al. [9] showed that a granular sample resists better shearing if the particle rotation is prohibited or reduced.

The partial stresses $\widehat{\boldsymbol{\sigma}}^F$ and $\widehat{\boldsymbol{\sigma}}^C$ defined in (5) give the contribution of each fraction to the macroscopic stress. If the solid fraction was homogeneous, the contribution of the fine fraction would be proportional to fine content f_c, e.g. 40% of fine content would contribute to 40% of the macroscopic stress. Figure 15 shows that the contribution of the fine fraction to the macroscopic stress is far from being proportional

Fig. 14 A granular binary mixture is assimilated to a system of gears. Black and gray gears correspond to particles included in the strong and weak force networks, respectively
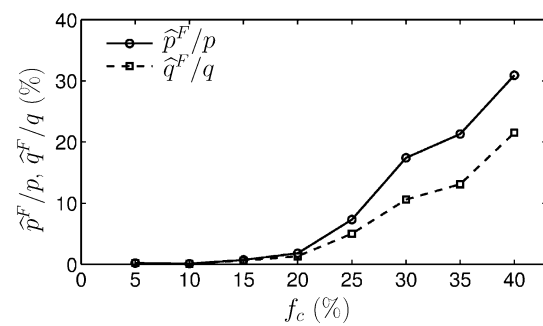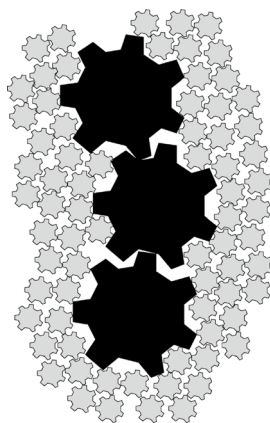

Fig. 15 Contributions of the fine fraction to the macroscopic mean and deviatoric stresses, p and q, at the peak state versus fine content f_c

to fine content f_c. The fine particles do not significantly contribute to the macroscopic stress when $f_c < 20\%$ but they do when $f_c \geq 20\%$. Moreover, they contribute more to the mean stress p than to the deviatoric stress q: for $f_c = 40\%$, 21.5% of the deviatoric stress q is provided by the fine particles, which is much lower than the value of 30.9% of the mean stress p. It can be concluded that for the studied range of fine content, the coarse particles play a primary role in carrying the shear stress, while the fine particles play the role of a matrix that reinforces the coarse ones.

5 Classification of granular mixtures

According to Thevanayagam et al. [7], the micro-structure of granular mixtures can be constituted in many different ways, depending on fine content. The authors proposed three limiting categories of micro-structure: (a) the coarse–coarse contacts are dominant, (b) the fine–fine contacts are dominant, and (c) the fine and coarse particles form a layered system. The current study brought several interesting insights into the variation of the granular micro-structure and how the coarse–coarse, coarse–fine and fine–fine contacts participate in sustaining the shear stress, depending on fine content. It turns out that the fine–coarse contacts play an important role in the micro-structure and there exists an intermediate category between (a) and (b), where these contacts primarily bear the shear stress. We propose, therefore, the following classification of granular mixtures into four limiting categories of micro-structure with three threshold values as illustrated in Fig. 16.

- Category (i) for $f_c < f_{c,1}^{\text{th}}$: the fine particles are almost floating within intercoarse voids, hence they have a little contribution to supporting the shear stress. The shear strength is then not affected by fine content.
- Category (ii) for $f_{c,1}^{\text{th}} \leq f_c < f_{c,2}^{\text{th}}$: the fine particles partially fill intercoarse voids but they partially separate coarse

Fig. 16 Four categories of micro-structure for granular gap-graded soils
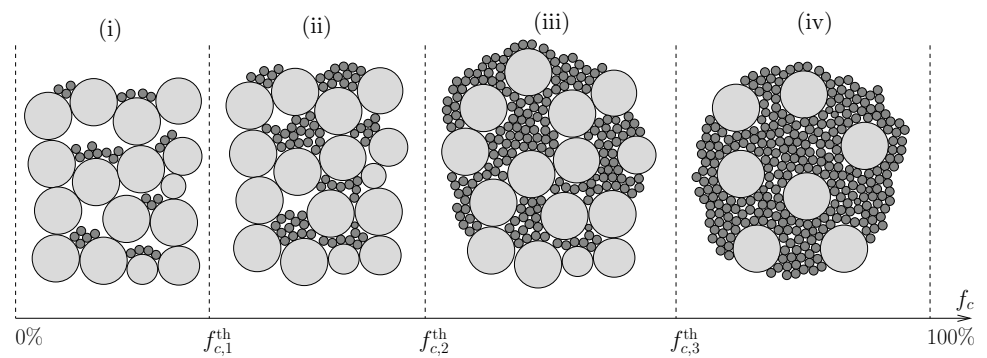
ones. The fine–coarse contacts are created and contribute to carrying the shear stress. However, contacts between coarse particles primarily carry the shear stress. In this case, the shear strength increases with fine content.

- Category (iii) for $f_{c,2}^{\text{th}} \leq f_c < f_{c,3}^{\text{th}}$: the fine particles fully fill intercoarse voids and greatly destroy coarse–coarse contacts. The fine–fine contacts participate in carrying the shear stress. The major contribution to the shear stress is provided by the fine–coarse contacts. In this case, the shear strength decreases with fine content.

- Category (iv) for $f_c \geq f_{c,3}^{\text{th}}$: the coarse particles are fully dispersed by the fine ones. The behavior of granular mixtures of this category is mainly governed by the fine particles. It is thus expected that the shear strength is independent of fine content in this case.

It is should be noted that this classification does not include the category (c) of layered micro-structure considered by Thevanayagam et al. For the binary mixtures considered in our study, the first and second threshold values, $f_{c,1}^{\text{th}}$ and $f_{c,2}^{\text{th}}$, are about 20% and 30%, respectively. We could not determine the third threshold value $f_{c,3}^{\text{th}}$ since the computation time for simulating binary mixtures with very high fine content is too long. It is worth mentioning that these threshold values might depend on many factors like the gap ratio, the particle shape or the sample density. According to Minh et al. [11], the last threshold value $f_{c,3}^{\text{th}}$ is about 60% for binary mixtures under one-dimensional compression with a gap ratio about 4.0.

6 Conclusions

In this paper, we have presented a study on the effect of fine content on the mechanical behavior of granular gap-graded materials subjected to shear loading. Numerical samples composed of fine and coarse spherical particles with different fine contents up to 40% are simulated using the DEM. Triaxial compression tests are then performed on these samples and their behavior is investigated at the macro- and micro-scales. This study brought a lot of insights into the granular micro-structure and the stress transmission in granular mixtures, which allowed us to explain why the fine particles can have no effect, positive effect or negative effect on their stress-strain behavior, depending on fine content. At a low fine content ($f_c < 20\%$), the fine particles are almost floating within the void space between the coarse particles so they do not participate significantly in carrying the shear stress. Starting from 20% of fine content, the fine particles cause two opposite effects to the granular micro-structure: on one hand, they come into contact with coarse particles and reinforce the micro-structure, but on the other hand, they separate coarse particles and then weaken the micro-structure. As a consequence, the shear stress is transmitted more and more through the coarse–fine contacts but less and less through the coarse–coarse contacts as fine content increases. The optimal fine content is about 30% under which the coarse–coarse contacts primarily support the shear stress. A decrease in the stress part carried by them is compensated by a strong increase in the stress part carried by the coarse–fine contacts. As a result, the shear strength increases with fine content. Above this optimal fine content, the coarse–fine contacts overtake the coarse–coarse contacts in carrying the shear stress. The coarse fraction is greatly weakened and is not sufficiently reinforced by the coarse–fine contacts, hence the shear strength decreases. For the studied range of fine content, the fine–fine contacts have little contribution to the macro-stress. It was also found that the strong force network in the studied granular mixtures includes almost all the coarse–coarse contacts but no more than 50% of coarse–fine contacts. Furthermore, a major fraction of fine–fine contacts are located in the weak force network.

For the studied range of fine content, the coarse particles constitute primarily the solid skeleton to resist the shear loading, leaving the fine particles under lower stresses. Interestingly, the role of the fine particles is more important in carrying the mean stress than in carrying the deviatoric stress. At a high fine content, the fine fraction suffers a marked softening phase after the peak state.

Based on this study, a classification of binary mixtures into four limiting categories of micro-structure was proposed. The particularity of the proposed classification is that it considers the importance of the coarse–fine contacts in the micro-structure. When fine content exceeds a threshold value (about 30% in our simulations), these contacts overtake the coarse–coarse contacts in carrying the shear stress.

Compliance with ethical standards

Conflict of interest The authors declare that they have no conflict of interest.

References

1. Sail, Y., Marot, D., Sibille, L., Alexis, A.: Suffusion tests on cohesionless granular matter. Eur. J. Environ. Civ. Eng. **15**(5), 799–817 (2011)
2. Ke, L., Takahashi, A.: Strength reduction of cohesionless soil due to internal erosion induced by one-dimensional upward seepage flow. Soils Found. **52**(4), 698–711 (2012)
3. Ke, L., Takahashi, A.: Triaxial erosion test for evaluation of mechanical consequences of internal erosion. Geotech. Test. J. **37**(2), 347–364 (2014)
4. Murthy, T., Loukidis, D., Carraro, J., Prezzi, M., Salgado, R.: Undrained monotonic response of clean and silty sands. Géotechnique **57**(3), 273–288 (2007)
5. Nguyen, T., Benahmed, N., Hicher, P.Y., Nicolas, M.: The influence of fines content on the onset of instability and critical state line of silty sand. In: Chau, K.T., Zhao, J. (eds.) Bifurcation and Degradation of Geomaterials in the New Millennium, IWBDG 2014, Springer Series in Geomechanics and Geoengineering, pp. 113–120. Springer, Cham (2015)
6. Salgado, R., Bandini, P., Karim, A.: Shear strength and stiffness of silty sand. J. Geotech. Geoenviron. Eng. **126**(5), 451–462 (2000)
7. Thevanayagam, S., Shenthan, T., Mohan, S., Liang, J.: Undrained fragility of clean sands, silty sands, and sandy silts. J. Geotech. Geoenviron. Eng. **128**(10), 849–859 (2002)
8. Kim, F., Penumadu, D., Gregor, J., Kardjilov, N., Manke, I.: High-resolution neutron and X-ray imaging of granular materials. J. Geotech. Geoenviron. Eng. **139**(5), 715–723 (2012)
9. Belheine, N., Plassiard, J., Donzé, F., Darve, F., Seridi, A.: Numerical simulation of drained triaxial test using 3D discrete element modeling. Comput. Geotech. **36**(1), 320–331 (2009)
10. Minh, N., Cheng, Y.: On the contact force distributions of granular mixtures under 1D-compression. Granul. Matter **18**(2), 1–12 (2016)
11. Minh, N., Cheng, Y., Thornton, C.: Strong force networks in granular mixtures. Granul. Matter **16**(1), 69–78 (2014)
12. Shire, T., O'Sullivan, C.: Micromechanical assessment of an internal stability criterion. Acta Geotech. **8**(1), 81–90 (2013)
13. Shire, T., O'Sullivan, C., Hanley, K.: The influence of fines content and size-ratio on the micro-scale properties of dense bimodal materials. Granul. Matter **18**(3), 1–10 (2016)
14. Voivret, C., Radjai, F., Delenne, J.Y., El Youssoufi, M.: Multiscale force networks in highly polydisperse granular media. Phys. Rev. Lett. **102**(17), 178001 (2009)
15. Dai, B., Yang, J., Luo, X.: A numerical analysis of the shear behavior of granular soil with fines. Particuology **21**, 160–172 (2015)
16. Ng, T.T., Zhou, W., Chang, X.L.: Effect of particle shape and fine content on the behavior of binary mixture. J. Eng. Mech. **143**(1), C4016008-1–C4016008-9 (2016)
17. Aboul-Hosn, R.: Suffusion and its effects on the mechanical behavior of granular soils: numerical and experimental investigations. Ph.D. thesis, Université Grenoble Alpes (2016)
18. Luding, S.: Introduction to discrete element methods: basic of contact force models and how to perform the micro-macro transition to continuum theory. Eur. J. Environ. Civ. Eng. **12**(7–8), 785–826 (2008)
19. Radjai, F., Richefeu, V.: Contact dynamics as a nonsmooth discrete element method. Mech. Mater. **41**(6), 715–728 (2009)
20. Šmilauer, V., et al.: Yade Documentation 2nd ed. The Yade Project (2015). https://doi.org/10.5281/zenodo.34073. http://yade-dem.org/doc/
21. Scholtès, L., Hicher, P.Y., Sibille, L.: Multiscale approaches to describe mechanical responses induced by particle removal in granular materials. Comptes Rendus Mécanique **338**(10–11), 627–638 (2010)
22. Chang, D., Zhang, L.: Extended internal stability criteria for soils under seepage. Soils Found. **53**(4), 569–583 (2013)
23. Thevanayagam, S., Mohan, S.: Intergranular state variables and stress-strain behaviour of silty sands. Géotechnique **50**(1), 1–23 (2000)
24. ASTM D4767–88.: Standard test method for consolidated-undrained triaxial compression test on cohesive soils. Standard ASTM 04.08 (1988)
25. NF P 94-074: Sols.: reconnaissances et essais—Essais à l'appareil triaxial de révolution. AFNOR (Association Français de Normalisation) (1994)
26. Wiącek, J., Molenda, M.: Representative elementary volume analysis of polydisperse granular packings using discrete element method. Particuology **27**, 88–94 (2016)
27. Salot, C., Gotteland, P., Villard, P.: Influence of relative density on granular materials behavior: DEM simulations of triaxial tests. Granul. Matter **11**(4), 221–236 (2009)
28. Shire, T., O'Sullivan, C., Hanley, K., Fannin, R.: Fabric and effective stress distribution in internally unstable soils. J. Geotech. Geoenviron. Eng. **140**(12), 04014072-1–04014072-11 (2014)
29. Chareyre, B.: Modélisation du comportement d'ouvrages composites sol-géosynthétique par éléments discrets: application aux ancrages en tranchées en tête de talus. Ph.D. thesis, Université Grenoble I-Joseph Fourrier (2003)
30. Skempton, A., Brogan, J.: Experiments on piping in sandy gravels. Géotechnique **44**(3), 449–460 (1994)
31. Lade, P., Liggio, C., Yamamuro, J.: Effects of non-plastic fines on minimum and maximum void ratios of sand. Geotech. Test. J. **21**(4), 336–347 (1998)
32. Holtzman, R., Silin, D., Patzek, T.: Mechanical properties of granular materials: a variational approach to grain-scale simulations. Int. J. Numer. Anal. Meth. Geomech. **33**(3), 391–404 (2009)
33. Suiker, A., Fleck, N.: Frictional collapse of granular assemblies. J. Appl. Mech. **71**(3), 350–358 (2004)
34. Yan, G., Yu, H.S., McDowell, G.: Simulation of granular material behaviour using DEM. Proc. Earth Planet. Sci. **1**(1), 598–605 (2009)

35. Yang, Z., Yang, J., Wang, L.: On the influence of inter-particle friction and dilatancy in granular materials: a numerical analysis. Granul. Matter **14**(3), 433–447 (2012)

36. Minh, N., Cheng, Y.: A DEM investigation of the effect of particle-size distribution on one-dimensional compression. Géotechnique **63**, 44–53 (2013)

37. Shire, T., O'Sullivan, C., Hanley, K.: The influence of finer fraction and size-ratio on the micro-scale properties of dense bimodal materials. In: Soga, K., Kumar, K., Biscontin, G., Kuo, M. (eds.) Proceedings of the TC105 ISSMGE International Symposium on Geomechanics from Micro to Macro, pp. 231–236, Cambridge, UK, September 2014.

38. Radjai, F., Wolf, D.: Features of static pressure in dense granular media. Granul. Matter **1**(1), 3–8 (1998)

39. Thornton, C.: Force transmission in granular media. KONA Powder Parti. J. **15**, 81–90 (1997)

40. Christoffersen, J., Mehrabadi, M., Nemat-Nasser, S.: A micromechanical description of granular material behavior. J. Appl. Mech. **48**(2), 339–344 (1981)

41. Moreau, J.: Numerical investigation of shear zones in granular materials. In: Wolf, D.E., Grassberger, P. (eds.) Friction, Arching, Contact Dynamics, pp. 233–247, World Scientific, Singapore (1997)

42. Staron, L., Radjai, F., Vilotte, J.: Multi-scale analysis of the stress state in a granular slope in transition to failure. Eur. Phys. J. E Soft Matter Biol. Phys. **18**(3), 311–320 (2005)

43. Calvetti, F., Viggiani, G., Tamagnini, C.: A numerical investigation of the incremental behavior of granular soils. Rivista Italiana Di Geotecnica **3**, 11–29 (2003)